Published in final edited form as:
Gene. 2014 April 1; 538(2): 328–333. doi:10.1016/j.gene.2014.01.009.

Altered gene dosage confirms the genetic interaction between FIAT and αNAC

Bahareh Hekmatnejad[1,2], **Vice Mandic**[1,2], **Vionnie W.C. Yu**[1,2,3], **Omar Akhouayri**[1,2,4], **Alice Arabian**[1], and **René St-Arnaud**[1,2,5,6]

[1]Research Unit, Shriners Hospital for Children - Canada, Montreal (Quebec) Canada H3G 1A6

[2]Department of Human Genetics, McGill University, Montreal, (Quebec) Canada H3A 2T5

[5]Departments of Surgery and Medicine, McGill University, Montreal, (Quebec) Canada H3A 2T5

Abstract

Factor inhibiting ATF4-mediated transcription (FIAT) interacts with Nascent polypeptide associated complex And coregulator alpha (αNAC). In cultured osteoblastic cells, this interaction contributes to maximal FIAT-mediated inhibition of *Osteocalcin* (*Ocn*) gene transcription. We set out to demonstrate the physiological relevance of this interaction by altering gene dosage in compound *Fiat* and *Naca* (encoding αNAC) heterozygous mice. Compound $Naca^{+/-}; Fiat^{+/-}$ heterozygous animals were viable, developed normally, and exhibited no significant difference in body weight compared with control littermate genotypes. Animals with a single *Fiat* allele had reduced *Fiat* mRNA expression without changes in the expression of related family members. Expression of the osteocyte differentiation marker *Dmp1* was elevated in compound heterozygotes. Static histomorphometry parameters were assessed at 8 weeks of age using microcomputed tomography (μCT). Trabecular measurements were not different between genotypes. Cortical thickness and area were not affected by gene dosage, but we measured a significant increase in cortical porosity in compound heterozygous mice, without changes in biomechanical parameters. The bone phenotype of compound $Naca^{+/-}; Fiat^{+/-}$ heterozygotes confirms that FIAT and αNAC are part of a common genetic pathway and support a role for the FIAT/αNAC interaction in normal bone physiology.

Keywords

Factor Inhibiting ATF4-mediated Transcription (FIAT); Nascent polypeptide associated complex And Coregulator alpha (αNAC); Bone; Cortical porosity

1. INTRODUCTION

The leucine zipper protein, FIAT (Factor Inhibiting ATF4-mediated Transcription), forms inactive heterodimers with the transcription factor ATF4 and inhibits its binding to DNA

[6]Address Correspondence to: René St-Arnaud, Research Unit, Shriners Hospital for Children – Canada, 1529 Cedar Avenue, Montreal (Quebec) Canada H3G 1A6, Tel: (514) 282-7155, Fax: (514) 842-5581, rst-arnaud@shriners.mcgill.ca.
[3]Current address: Harvard Stem Cell Institute, Massachusetts General Hospital, Boston, MA 02114
[4]Current address: Laboratoire de Génétique – Neuroendocrinologie et Biotechnologie, Faculté des Sciences Ibn Tofaïl, Kénitra, Morocco

(Yu et al., 2005; Yu et al., 2008). Because ATF4 is a key regulator of osteoblast biology (Yang et al., 2004), the net result of the binding of FIAT to ATF4 is an inhibition of osteoblast function. Over-expressing FIAT in osteoblasts of transgenic mice leads to reduced *Osteocalcin* (*Ocn*) gene transcription and osteopenia with reduced bone mineral density, lowered trabecular volume, and decreased bone strength (Yu et al., 2005). Reciprocally, inhibition of *Fiat* expression using siRNA-mediated knockdown leads to increased ATF4 activity and results in higher *Ocn* transcription, type I collagen synthesis, and mineralization (Yu et al., 2009b).

FIAT was initially cloned using a yeast two-hybrid screen for proteins interacting with αNAC (Nascent polypeptide associated complex And Coregulator alpha, encoded by the *Naca* gene), a transcriptional coregulator of gene expression in bone cells (Akhouayri et al., 2005; Yu et al., 2005; Yu et al., 2006; Meury et al., 2010). This interaction was independently confirmed using over-expression of epitope-tagged proteins in heterologous cell systems (Yoshida et al., 2005). Our recent work has confirmed that endogenous, post-translationally modified αNAC functionally interacts with the FIAT protein in osteoblastic cells to maximally repress ATF4-mediated *Ocn* gene transcription (Hekmatnejad et al., 2014). We set out to provide evidence of the physiological relevance of these findings through manipulation of *Fiat* and *Naca* dosage in genetically modified mice, with particular focus on skeletal development.

The *Fiat* gene (NM_178935.4) is located on the X chromosome and is ubiquitously expressed at the mRNA level (Nogami et al., 2004), but its protein expression pattern has only been studied extensively in bone cells (Yu et al., 2009a). The *Fiat* gene, like the majority of X-linked genes, is subject to random inactivation of one allele in females (Lyon, 1999). Therefore, approximately 50% of the cells in *Fiat* mutant heterozygotes should express the mutant allele, and the other half express normal allele. The *Naca* gene (NC_000076.6) maps to chromosome 10 (Yotov and St-Arnaud, 1996b) and encodes the related proteins αNAC and skNAC through differential splicing of its large third exon (Yotov and St-Arnaud, 1996a). Global targeting of the *Naca* gene in conventional knockout mice results in early embryonic lethality (Akhouayri et al., unpublished), and we had to use knock-in mutagenesis to confirm the physiological role of αNAC in bone tissue (Meury et al., 2010). However, mice heterozygous for the conventional *Naca* knockout mutation have no detectable phenotype and their skeletal development is normal (Pellicelli et al., submitted), therefore allowing gene dosage alteration in compound heterozygous animals.

We crossed heterozygous *Fiat*-deficient mice with heterozygous *Naca*-deficient mice to generate double heterozygous *Naca* and *Fiat* female mice. Femoral bone microstructure was examined using microcomputed tomography (μCT). While trabecular bone was not affected by altered gene dosage for *Naca* and *Fiat*, compound $Naca^{+/-}$; $Fiat^{+/-}$ heterozygous mice displayed significantly higher cortical porosity with increased expression of the osteocyte differentiation marker, *Dentin matrix protein-1* (*Dmp1*). This phenotype confirms that FIAT and αNAC are part of a common genetic pathway and supports a role for FIAT/αNAC interactions in bone physiology.

2. MATERIALS and METHODS

2.1 Generation of *Naca; Fiat* Compound Heterozygous Mutant Mice

A 9.6 kb genomic fragment spanning the 5′ UTR, exon 1, and the first intron of the mouse *Fiat* allele was used in the construction of the targeting vector (Fig 1A). A 34 bp LoxP sequence was inserted upstream from exon 1 and a 6.4 kb PGK-neo-HsvTK cassette flanked by two LoxP sites was introduced within intron 1. The backbone vector was pBluescript. The targeting vector was linearized and electroporated into R1 embryonic stem (ES) cells

(Nagy et al., 1993) that were subsequently cultured in the presence of G418. Positive clones were identified using Southern blotting and PCR. Blastocyst injection into C57BL/6 was performed according to standard protocols (Hogan et al., 1994). Chimeras were bred with a general deleter Cre transgenic strain (CMV-Cre) (Su et al., 2002) to delete the selection cassette.

The αNAC targeting vector was constructed using a genomic *Naca* clone (Meury et al., 2010) by inserting an IRES-LacZ-Neo cassette at the start codon within exon 2 to create a null allele (Fig. 1B). Gene targeting and production of chimeric mice were performed according to standard protocols (Hogan et al., 1994).

All animal procedures were reviewed and approved by the McGill Institutional Animal Care and Use Committee and followed the guidelines of the Canadian Council on Animal Care. Mice were kept in an environmentally controlled barrier animal facility with a 12-hour light, 12-hour dark cycle and were fed mouse chow and water ad libitum. $Naca^{+/-}$ males were crossed to $Fiat^{+/-}$ females to obtain control ($Naca^{+/+}$; $Fiat^{+/+}$, $Naca^{+/-}$; $Fiat^{+/+}$, $Naca^{+/+}$; $Fiat^{+/-}$) and test ($Naca^{+/-}$; $Fiat^{+/-}$) genotypes.

2.2 Genotyping

Initial homologous recombination in ES cells and germline transmission of the mutant *Naca* allele was confirmed using Southern blotting with diagnostic wild-type 8.5 kb and mutant 7.6 kb XbaI restriction fragments (Fig. 1B). For subsequent routine genotyping, DNA was prepared from tail snips (Laird et al., 1991) and analyzed in two independent polymerase chain reactions (PCR) for the presence of the *Fiat* and *Naca* wild-type and targeted alleles. For each allele, three primers were used.

Fiat primers: 5′-TGAATAGGCTTCCAGCCCAAAGG-3′; 5′-CCAAGAGTCCCAAAAGAGCATG-3′, 5′-CCTTCTGGGGCTTGTAGTCTC-3′. *Naca* primers: 5′-GTGTTCGAATTGGCCAATGACAAGAC-3′, 5′-CTTTCTTCCCCGAAGAGTCCC-3′, 5′-TCGGAATACTTAGACTAGGCGGA-3′.

2.3 Real-time Reverse Transcription quantitative PCR (RT-qPCR)

Calvaria from 8 week-old mice were collected into RNAlater solution (Ambion, Austin, TX) and were stored at −20°C until further processed. RNA was extracted with TRIzol (Invitrogen) following the manufacturer's instructions. One microgram of RNA was reverse-transcribed into cDNA using the High Capacity cDNA Archive Kit as per the manufacturer's recommendations (Applied Biosystems). Real-time PCR amplification was performed using the TaqMan® Universal PCR Master Mix (Applied Biosystems) on a 7500 instrument (Applied Biosystems) and specific Assay-On-demand TaqMan® assays for *Fiat*, *α-taxilin*, *β-taxilin*, *Naca*, *Ocn*, and *Dentin matrix protein-1* (*Dmp1*). Relative quantification of mRNA was performed according to the comparative C_t method with 18S ribosomal RNA as endogenous control (ABI PRISM 7700 Sequence Detector User Bulletin [2], PE Applied Biosystems 1997). Fourteen to sixteen samples per genotype were assayed in duplicates.

2.4 Sample preparation

Femurs were collected and cleaned of soft tissue, fixed overnight in 4% paraformaldehyde, washed with 1X phosphate buffer saline, and dehydrated in 50%, then 70% ethanol. Samples were stored in 70% ethanol at 4 °C until scanning.

2.5 Static histomorphometry

Microcomputed tomography was performed using the SkyScan/Bruker 1172 high-resolution μCT scanner of the McGill University Health Center Orthopaedic Research division. The

parameters were 5 μm pixel size, 50 kV, 194 μA, 0.5 mm Al filter, angular rotation step of 0.45°, and an exposure time of 500 ms with a total scan duration of 45min. Three-frame averaging was used to improve the signal-to-noise ratio. After scanning, 3D microstructural image data was reconstructed using the manufacturer's software (Skyscan NRecon). The ring artifact correction was 4 and the beam hardening correction was set at 30%.

Structural indices were calculated using Skyscan CT Analyzer (CTAn) software. The regions of interest (ROIs) for trabecular microarchitectural variables was defined starting at 0.639 mm proximal to the growth plate of each femur and extending 1.475 mm in the direction of the diaphysis where trabeculae were no longer visible. An upper threshold of 255 and a lower adaptive threshold of 50 were used to delineate each pixel as bone or non-bone and the following parameters were measured: tissue volume (TV, in mm^3), trabecular bone volume (BV, in mm^3), bone volume/tissue volume (BV/TV, %), trabecular number (1/mm), trabecular separation (in μm), trabecular thickness (in μm), structure model index (SMI), and connectivity density ($1/mm^3$).

To quantify cortical bone microstructure, ROI for each animal was chosen starting at 4.42 mm (900 lines, each line being 0.005 mm) distal to the growth plate and 1mm in height. Cortical bone measurements consisted of cross-sectional total and cortical area, cortical thickness, percent total cortical porosity, percent open porosity, and percent closed porosity.

2.6 Biomechanical parameters

In order to assess mechanical integrity, right femora were loaded to failure in a three-point bending assay using an Instron model 5943 single column table frame machine. Tests were carried out in the posterior-to-anterior direction at a loading rate of 0.05 mm/s and a support distance of 7mm. From the resulting load vs. displacement curves, structural properties were calculated to describe the specific aspects of the tissue's mechanical behavior under load. Those properties included stiffness (N/mm), maximum force at failure (N), displacement at maximum force (mm), and maximum displacement at failure/ultimate displacement (mm). Stiffness was defined as the slope of the elastic portion of the load/displacement curve and the maximum force was defined as the largest load value registered during the tests.

2.7 Statistical analysis

Kolmogorov-Smirnov tests were employed to confirm normal distribution of the variables in each dataset. Data were expressed as mean ± S.E.M. Statistical differences were calculated using Student's *t*-test or Analysis of Variance with posthoc tests. $P<0.05$ was accepted as statistically significant.

3. RESULTS

3.1 Gross phenotype

Female mice of all control genotypes ($Naca^{+/+}$; $Fiat^{+/+}$, $Naca^{+/-}$; $Fiat^{+/+}$, $Naca^{+/+}$; $Fiat^{+/-}$) and compound heterozygous ($Naca^{+/-}$; $Fiat^{+/-}$) mice were viable and born at the expected Mendelian ratio. Mice developed normally and exhibited no obvious behavioral or physical phenotype. Furthermore, $Naca^{+/-}$; $Fiat^{+/-}$ compound heterozygous female mice fed on a regular diet showed no differences in size or body weight when compared with control littermate genotypes, at birth or up to 8 weeks of age (Fig. 2 and data not shown).

3.2 Gene expression monitoring

Animals with a single *Fiat* allele had reduced *Fiat* mRNA expression without changes in the expression of the related family members, *α-taxilin* and *β-taxilin* (Nogami et al., 2004) (Fig. 3A–C). We did not measure an impact of *Naca* gene dosage on *Naca* expression (Fig. 3D).

Surprisingly, the mRNA levels of the best characterized transcriptional target of FIAT and αNAC, *Ocn*, were not affected when one allele of either or both genes, *Fiat* and *Naca*, were inactivated (Fig. 3E). However, expression of the osteocyte differentiation marker *Dmp1* was increased in $Naca^{+/-}$; $Fiat^{+/-}$ compound heterozygotes (Fig. 3F).

3.3 Absence of trabecular phenotype

To evaluate bone structural histology, femurs from compound heterozygous and control females were compared by 3D analysis using μCT. Trabecular histomorphometric parameters were evaluated at the distal metaphysis. There were no significant effect of heterozygous *Naca* and *Fiat* deficiency on trabecular bone volume, number, thickness, or separation and other trabecular parameters assessed for any of the genotypes (Table 1).

3.4 Cortical phenotype

Microcomputed tomography measurements of cortical bone from the femoral mid-diaphysis revealed that the mean values of cortical traits (area, total cross-sectional area within the periosteal envelope, and cortical thickness) were statistically indistinguishable in both control and compound heterozygous mice (Table 1). On visual assessment, cortical porosity appeared increased when one copy of *Naca* and one copy of *Fiat* were inactivated (compare panels A and B, Fig. 4). Since values for all control genotypes ($Naca^{+/+}$; $Fiat^{+/+}$, $Naca^{+/-}$; $Fiat^{+/+}$, $Naca^{+/+}$; $Fiat^{+/-}$) were highly homogeneous, results from these animals were grouped and expressed as 'Control' to increase statistical power. Total cortical porosity was significantly increased in mice heterozygous for both *Naca* and *Fiat* (Fig. 4C). When open and closed porosity were analyzed separately, percent closed porosity, reflecting osteocyte lacunae and intracortical resorption, was significantly higher in $Naca^{+/-}$; $Fiat^{+/-}$ mice when compared to control genotypes (Fig. 4D). In addition, percent open porosity, reflecting vascular canals, was augmented in bones of compound heterozygous mice (Fig. 4E).

3.5 Biomechanical properties

We next analyzed whether the increased cortical porosity measured in mice with altered *Naca* and *Fiat* gene dosage leads to a decreased biomechanical stability. Mechanical testing of femurs via three-point bending revealed no differences in stiffness and strength between compound heterozygotes and controls. In addition, there was no difference in ultimate displacement or displacement at maximum force (Fig 5).

4. DISCUSSION

We previously confirmed the interaction of endogenous FIAT and αNAC proteins in osteoblasts and demonstrated a functional role for this interaction in osteoblast function, related to maximal repression of ATF4-mediated transcription of the *Ocn* gene (Hekmatnejad et al., 2014). In the present study, we attempted to assess the physiological relevance of the interaction between αNAC and FIAT by creating a mouse model of combined *Fiat* and *Naca* heterozygous deficiency. Gene dosage alteration is often used to provide evidence that proteins are part of common genetic pathways (Yang et al., 2004; Lee et al., 2007; Ferron et al., 2010; Oury et al., 2011). Compound heterozygous ablation of *Naca* and *Fiat* resulted in an increase in cortical porosity, which included both open and closed porosity. This bone phenotype confirms that FIAT and αNAC are part of a common genetic pathway and support a role for the FIAT/αNAC interaction in normal bone physiology.

There are several types of porosity in cortical bone (Cowin et al., 2009). Resorption cavities, ranging from 50 μm to 300 μm, can be observed during bone remodeling. The vascular porosity, which consists of the column of all the tunnels in bone that contain blood vessels

and includes all the primary and secondary osteonal canals as well as transverse (Volkmann) canals, is measured in the order of 10–20 μm in diameter. Lacunae-canaliculae porosity is associated with osteocyte lacunae (10–20 μm) and canaliculi channels (in the 100 nm range). Finally, the smallest pore size in bone is associated with the collagen-apatite porosity. These pores are found between the collagen fibers and apatite crystals and average 40 nm. Vascular porosity in mice tissue has been reported at a value range of 1–5% while the lacunar-canalicular porosity accounts for ~1% of the bone tissue (Cardoso et al., 2013). Our preferred interpretation of the increased porosity in *Naca*$^{+/-}$; *Fiat*$^{+/-}$ mice is that lacunar-canalicular porosity was increased. This is based on the emerging evidence that impaired αNAC nuclear activity affects osteoblast maturation and osteocyte number *in vivo* (Meury et al., 2010; Pellicelli et al., submitted). Mice with a knock-in mutation that reduces the nuclear translocation of αNAC have osteopenia with a reduced volume of immature, woven-type bone characterized by an increase in the number of osteocytes (Meury et al., 2010). In addition, FIAT protein expression has been localized to osteocytes in adult mice (Yu et al., 2009a). Reduced αNAC and/or FIAT expression or activity in compound heterozygous mice could lead to increased osteocyte numbers, which would translate into increased cortical porosity due to a larger number of lacunae and canaliculae. This hypothesis is supported by the measured elevated expression of the osteocyte differentiation marker, *Dmp1*, in *Naca*$^{+/-}$; *Fiat*$^{+/-}$ mice (Fig. 3F).

Recent studies have indicated that osteocytes are an essential source of RANKL for osteoclast formation (Xiong et al., 2011). Thus, osteocytes have the ability to independently regulate the rate of bone remodeling (Xiong and O'Brien, 2012). It is thus also possible that the increased porosity of *Naca*$^{+/-}$; *Fiat*$^{+/-}$ compound heterozygous mice was due to increased osteoclastogenesis secondary to increased expression of RANKL in osteocytes. However, we did not detect any changes in *Rankl* mRNA expression or circulating RANKL concentrations in mice with reduced *Naca* and/or *Fiat* gene dosage (data not shown).

Cortical bone contributes significantly to the mechanical strength of bone (Mazess, 1990). Several studies have demonstrated the association between intracortical porosity and cortical bone strength and stiffness, and small changes in cortical porosity can lead to disproportionately substantial losses in bone strength (McCalden et al., 1993; Turner, 2002). It was thus surprising that the changes in cortical porosity measured in *Naca*$^{+/-}$; *Fiat*$^{+/-}$ mice were not accompanied by changes in biomechanical properties. Bone strength is determined by a large number of interrelated factors including the amount of bone, the spatial distribution of the bone mass, and the intrinsic properties of the materials that compromise the bone (Clarke, 2008). Therefore, investigation of these parameters in *Naca*$^{+/-}$; *Fiat*$^{+/-}$ mice could provide valuable insight as to the different roles that each plays with regard to skeletal bone quality.

Expression of *Ocn*, a transcriptional target of both αNAC and FIAT, was not affected by *Naca* or *Fiat* gene dosage alterations (Fig. 3E). Recent data highlight the key metabolic and developmental roles of OCN (Lee et al., 2007; Ferron et al., 2010; Oury et al., 2013). *Ocn* transcriptional regulation involves a large number of factors (reviewed in Jensen et al., 2010) that must provide redundancy to insure adequate *Ocn* expression under a myriad of genetic or physiological conditions. We surmise that one wild-type allele of *Naca* and *Fiat* help maintain homeotic *Ocn* expression as opposed to what is measured when all alleles of each gene are mutated (Meury et al., 2010; Hekmatnejad et al., unpublished observations).

Females singly heterozygous for *Fiat* (*Naca*$^{+/+}$; *Fiat*$^{+/-}$) had no discernable bone phenotype compared to wild-type *Naca*$^{+/+}$; *Fiat*$^{+/+}$ females despite reduced *Fiat* expression and X chromosome inactivation (XCI). The lack of *Fiat* gene dosage effect on bone phenotypic manifestations suggests that cells affected by the heterozygous *Fiat* mutation are actively

trying to maintain a similar activity level of FIAT as the wild-type ones. Potential mechanisms involve skewed X chromosome inactivation. In most females the number of cells with either X being active is roughly equal; however, skewing of X chromosome inactivation in a percentage of females can occur (Abkowitz et al., 1998). Some individuals may undergo skewed XCI by chance (random inactivation) or there may be factors controlling the initial choice of which X to inactivate, resulting in primary nonrandom inactivation (Minks et al., 2008). For instance, in mice the choice of chromosome inactivation involves the inactivation center, a region of the X chromosome that differs between strains and is necessary in *cis* for inactivation to occur (Heard et al., 1997). Therefore, we can propose that skewed X chromosome inactivation favors the cells with the normal *Fiat* allele thus influencing the phenotype of *Fiat* heterozygous female mice.

A number of factors could also have affected phenotypic manifestations in $Naca^{+/-}$; $Fiat^{+/-}$ compound heterozygous mice and explain the lack of impact of gene dosage alteration on trabecular bone. Redundancy of function caused by compensatory expression of *Fiat*-related family members (α- and β-taxilin) can be ruled out since their mRNA levels remained unchanged regardless of genotypes (Fig. 3B, C). However, functional redundancy could be achieved in bone through other family of proteins able to form inactive heterodimers with ATF4. Candidates include ICER (Chandhoke et al., 2008) or other leucine zipper factors such as CHOP (CCAAT/Enhancer-binding protein Homologous Protein) (Pereira et al., 2007). It is also possible that a stronger phenotype could be detected in older mice. Finally, a challenge to bone homeostasis could evoke a more pronounced phenotype. Experiments along those lines include the ovariectomized (OVX)/estrogen deficiency model of postmenopausal osteoporosis, fracture repair and/or distraction osteogenesis, or skeletal unloading.

At any rate, our results confirm that *Naca* and *Fiat* are part of a common genetic pathway. We are developing and characterizing additional mice models that will help to further understand the role of FIAT/αNAC interactions in bone physiology.

Acknowledgments

We thank Guylaine Bédard for preparing the figures. We used the microcomputed tomography instrument of the McGill University Health Center Orthopaedic Research Division and acknowledge support from the Network for Oral and Bone Health Research for access aid to this infrastructure. This work was supported by NIH grant AR53287 and by Shriners Hospitals for Children grant 86400 to R.St-A.

ABBREVIATIONS LIST

FIAT	Factor Inhibiting ATF4-mediated Transcription
αNAC	Nascent polypeptide associated complex And Coregulator alpha
Ocn	Osteocalcin
Dmp1	Dentin matrix protein-1
μCT	microcomputed tomography
ATF4	Activating Transcription Factor 4
siRNA	silencing ribonucleic acid
skNAC	skeletal isoform of αNAC
UTR	untranslated region

PGK-neo-HsvTk	phosphoglycerate kinase-neomycin-herpes simplex virus thymidine kinase
ES	embryonic stem
PCR	polymerase chain reaction
IRES-lacZ-neo	internal ribosome entry site-lacZ-neomycin
RT-qPCR	Reverse Transcription-quantitative Polymerase Chain Reaction
ROI	region of interest
TV	tissue volume
BV	bone volume
BV/TV	bone volume/tissue volume
SMI	structure model index
S.E.M	standard error of the mean
RANKL	receptor activating nuclear factor kappa ligand
XCI	X chromosome inactivation
ICER	inducible cAMP early repressor
CHOP	CCAAT/Enhancer-binding protein homologous protein
OVX	ovariectomized
Wt	wild-type
Mut	mutant

References

Abkowitz JL, Taboada M, Shelton GH, Catlin SN, Guttorp P, Kiklevich JV. An X chromosome gene regulates hematopoietic stem cell kinetics. Proc Natl Acad Sci USA. 1998; 95:3862–6. [PubMed: 9520458]

Akhouayri O, Quelo I, St-Arnaud R. Sequence-Specific DNA Binding by the alphaNAC Coactivator Is Required for Potentiation of c-Jun-Dependent Transcription of the Osteocalcin Gene. Mol Cell Biol. 2005; 25:3452–60. [PubMed: 15831452]

Cardoso L, Fritton SP, Gailani G, Benalla M, Cowin SC. Advances in assessment of bone porosity, permeability and interstitial fluid flow. J Biomech. 2013; 46:253–65. [PubMed: 23174418]

Chandhoke TK, Huang YF, Liu F, Gronowicz GA, Adams DJ, Harrison JR, Kream BE. Osteopenia in transgenic mice with osteoblast-targeted expression of the inducible cAMP early repressor. Bone. 2008; 43:101–9. [PubMed: 18460422]

Clarke B. Normal bone anatomy and physiology. Clin J Amer Soc Nephrol. 2008; 3(Suppl 3):S131–9. [PubMed: 18988698]

Cowin SC, Gailani G, Benalla M. Hierarchical poroelasticity: movement of interstitial fluid between porosity levels in bones. Phil Trans Series A, Math Phys Eng Sci. 2009; 367:3401–44.

Ferron M, Wei J, Yoshizawa T, Del Fattore A, DePinho RA, Teti A, Ducy P, Karsenty G. Insulin signaling in osteoblasts integrates bone remodeling and energy metabolism. Cell. 2010; 142:296–308. [PubMed: 20655470]

Heard E, Clerc P, Avner P. X-chromosome inactivation in mammals. Ann Rev Genet. 1997; 31:571–610. [PubMed: 9442908]

Hekmatnejad B, Akhouayri O, Jafarov T, St Arnaud R. SUMOylated alphaNAC potentiates transcriptional repression by FIAT. J Cell Biochem. 2014 in press.

Hogan, B.; Beddington, R.; Costantini, F.; Lacy, E. Manipulating the mouse embryo. A laboratory manual. 2. Cold Spring Harbor Laboratory Press; Cold Spring Harbor, NY: 1994.

Jensen ED, Gopalakrishnan R, Westendorf JJ. Regulation of gene expression in osteoblasts. Biofactors. 2010; 36:25–32. [PubMed: 20087883]

Laird PW, Zijderveld A, Linders K, Rudnicki MA, Jaenisch R, Berns A. Simplified mammalian DNA isolation procedure. Nucleic Acids Res. 1991; 19:4293. [PubMed: 1870982]

Lee NK, Sowa H, Hinoi E, Ferron M, Ahn JD, Confavreux C, Dacquin R, Mee PJ, McKee MD, Jung DY, Zhang Z, Kim JK, Mauvais-Jarvis F, Ducy P, Karsenty G. Endocrine regulation of energy metabolism by the skeleton. Cell. 2007; 130:456–69. [PubMed: 17693256]

Lyon MF. X-chromosome inactivation. Curr Biol. 1999; 9:R235–7. [PubMed: 10209128]

Mazess RB. Fracture risk: a role for compact bone. Calcif Tissue Int. 1990; 47:191–3. [PubMed: 2242490]

McCalden RW, McGeough JA, Barker MB, Court-Brown CM. Age-related changes in the tensile properties of cortical bone. The relative importance of changes in porosity, mineralization, and microstructure. J Bone Joint Surg. 1993; 75:1193–205. [PubMed: 8354678]

Meury T, Akhouayri O, Jafarov T, Mandic V, St-Arnaud R. Nuclear alpha NAC influences bone matrix mineralization and osteoblast maturation in vivo. Mol Cell Biol. 2010; 30:43–53. [PubMed: 19884350]

Minks J, Robinson WP, Brown CJ. A skewed view of X chromosome inactivation. J Clin Invest. 2008; 118:20–3. [PubMed: 18097476]

Nagy A, Rossant J, Nagy R, Abramow-Newerly W, Roder JC. Derivation of completely cell culture-derived mice from early-passage embryonic stem cells. Proc Natl Acad Sci USA. 1993; 90:8424–8. [PubMed: 8378314]

Nogami S, Satoh S, Tanaka-Nakadate S, Yoshida K, Nakano M, Terano A, Shirataki H. Identification and characterization of taxilin isoforms. Biochem Biophys Res Commun. 2004; 319:936–43. [PubMed: 15184072]

Oury F, Khrimian L, Denny CA, Gardin A, Chamouni A, Goeden N, Huang YY, Lee H, Srinivas P, Gao XB, Suyama S, Langer T, Mann JJ, Horvath TL, Bonnin A, Karsenty G. Maternal and offspring pools of osteocalcin influence brain development and functions. Cell. 2013; 155:228–41. [PubMed: 24074871]

Oury F, Sumara G, Sumara O, Ferron M, Chang H, Smith CE, Hermo L, Suarez S, Roth BL, Ducy P, Karsenty G. Endocrine regulation of male fertility by the skeleton. Cell. 2011; 144:796–809. [PubMed: 21333348]

Pereira RC, Stadmeyer LE, Smith DL, Rydziel S, Canalis E. CCAAT/Enhancer-binding protein homologous protein (CHOP) decreases bone formation and causes osteopenia. Bone. 2007; 40:619–626. [PubMed: 17095306]

Su H, Mills AA, Wang X, Bradley A. A targeted X-linked CMV-Cre line. Genesis. 2002; 32:187–8. [PubMed: 11857817]

Turner CH. Biomechanics of bone: determinants of skeletal fragility and bone quality. Osteoporosis Int. 2002; 13:97–104.

Xiong J, O'Brien CA. Osteocyte RANKL: new insights into the control of bone remodeling. J Bone Miner Res. 2012; 27:499–505. [PubMed: 22354849]

Xiong J, Onal M, Jilka RL, Weinstein RS, Manolagas SC, O'Brien CA. Matrix-embedded cells control osteoclast formation. Nature Med. 2011; 17:1235–41. [PubMed: 21909103]

Yang X, Matsuda K, Bialek P, Jacquot S, Masuoka HC, Schinke T, Li L, Brancorsini S, Sassone-Corsi P, Townes TM, Hanauer A, Karsenty G. ATF4 Is a Substrate of RSK2 and an Essential Regulator of Osteoblast Biology; Implication for Coffin-Lowry Syndrome. Cell. 2004; 117:387–98. [PubMed: 15109498]

Yoshida K, Nogami S, Satoh S, Tanaka-Nakadate S, Hiraishi H, Terano A, Shirataki H. Interaction of the taxilin family with the nascent polypeptide-associated complex that is involved in the transcriptional and translational processes. Genes Cells. 2005; 10:465–76. [PubMed: 15836775]

Yotov WV, St-Arnaud R. Differential splicing-in of a proline-rich exon converts alphaNAC into a muscle-specific transcription factor. Genes Dev. 1996a; 10:1763–72. [PubMed: 8698236]

Yotov WV, St-Arnaud R. Fine mapping of the alpha-NAC gene (Naca) to the distal end (D2–D3) of mouse chromosome 10. Mamm Genome. 1996b; 7:240. [PubMed: 8833254]

Yu VW, Akhouayri O, St-Arnaud R. FIAT is co-expressed with its dimerization target ATF4 in early osteoblasts, but not in osteocytes. Gene Expr Patterns. 2009a; 9:335–40. [PubMed: 19232401]

Yu VW, Ambartsoumian G, Verlinden L, Moir JM, Prud'homme J, Gauthier C, Roughley PJ, St-Arnaud R. FIAT represses ATF4-mediated transcription to regulate bone mass in transgenic mice. J Cell Biol. 2005; 169:591–601. [PubMed: 15911876]

Yu VW, El-Hoss J, St-Arnaud R. FIAT inhibition increases osteoblast activity by modulating Atf4-dependent functions. J Cell Biochem. 2009b; 106:186–92. [PubMed: 19016261]

Yu VW, Gauthier C, St-Arnaud R. Inhibition of ATF4 transcriptional activity by FIAT/gamma-taxilin modulates bone mass accrual. Ann NY Acad Sci. 2006; 1068:131–42. [PubMed: 16831913]

Yu VW, Gauthier C, St-Arnaud R. FIAT represses bone matrix mineralization by interacting with ATF4 through its second leucine zipper. J Cell Biochem. 2008; 105:859–865. [PubMed: 18680144]

HIGHLIGHTS

- We measured a significant increase in cortical porosity in *Naca*$^{+/-}$; *Fiat*$^{+/-}$ heterozygotes;
- Confirmation that FIAT and αNAC are part of a common genetic pathway;
- Results support a role for FIAT/αNAC interactions in bone physiology.

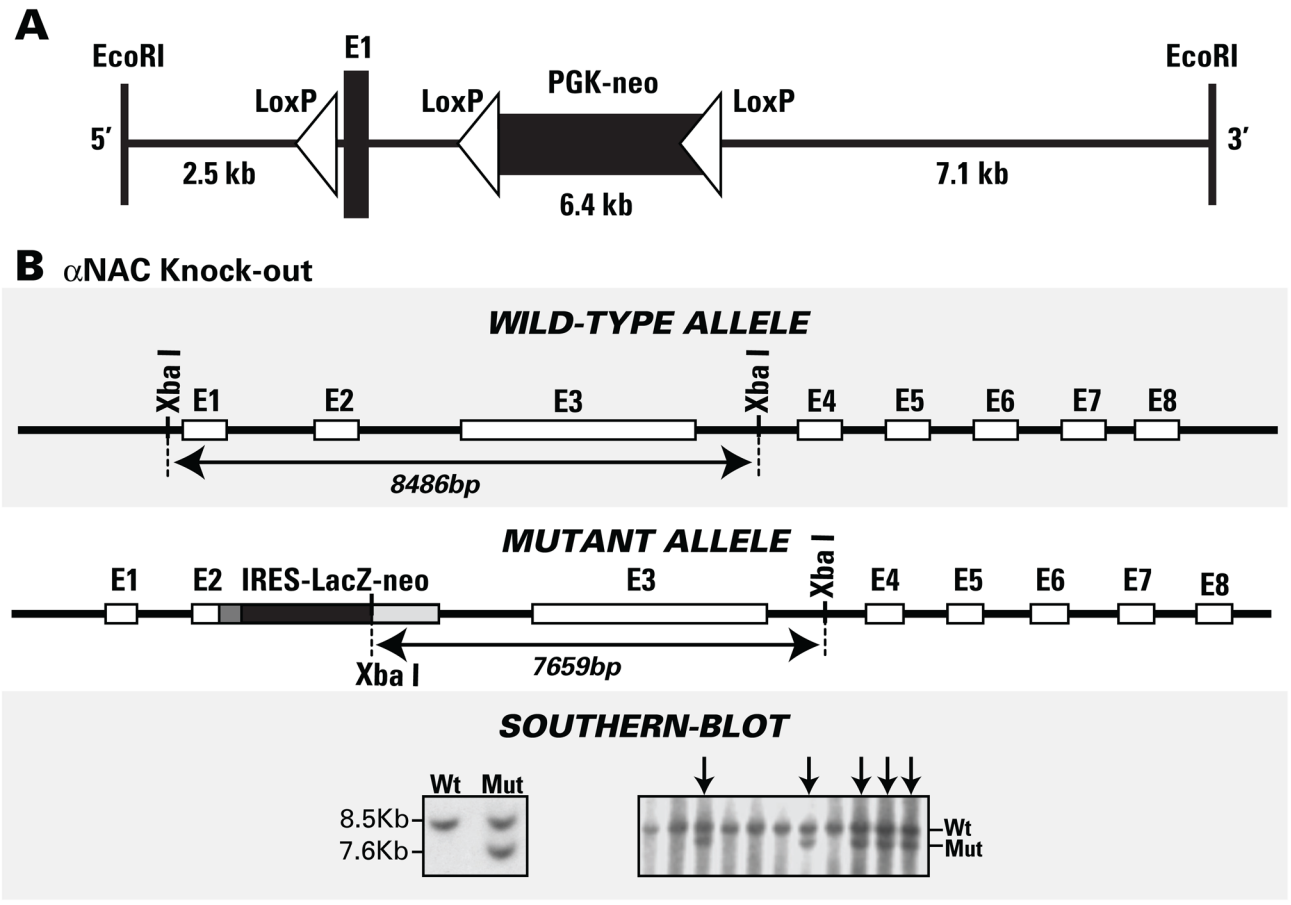

Fig. 1.

Targeted disruption of the murine *Fiat* and *Naca* genes by homologous recombination. A. *Fiat* targeting vector. A LoxP sequence (triangle) was inserted upstream from exon 1 and a PGK-neo cassette flanked by two LoxP sites was introduced within intron 1. B. Schematic drawing of the wild-type (Wt) and mutant (Mut) *Naca* alleles. An IRES-LacZ -neo cassette (gray-black box) was inserted at the ATG start site within exon 2. The diagnostic wild-type 8.5 kb and mutant 7.6 kb XbaI restriction fragments are indicated in the Southern blot from targeted ES cells (left) or tail snips from the first germline transmission litter.

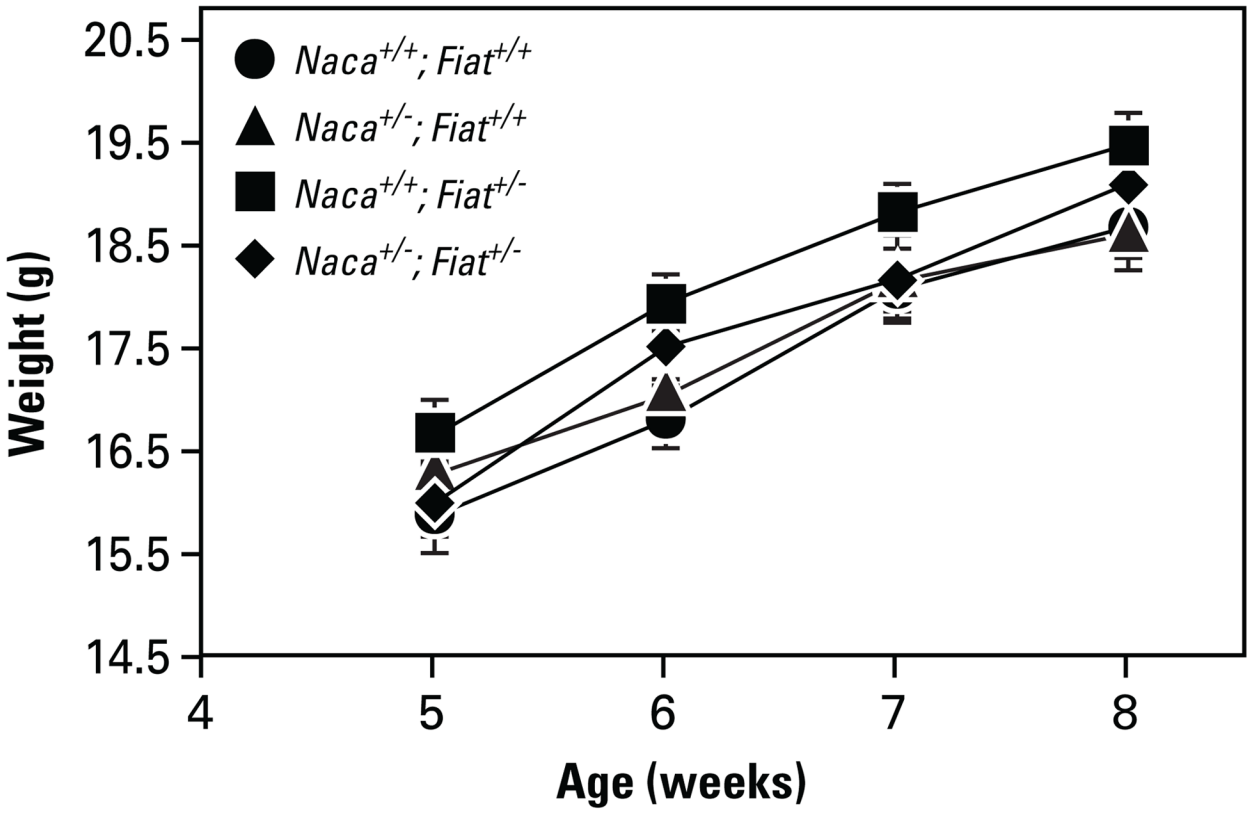

Fig. 2.

Fiat and *Naca* gene dosage alterations do not affect weight gain. No changes were observed between $Naca^{+/-}$; $Fiat^{+/-}$ compound heterozygous mice and control groups.

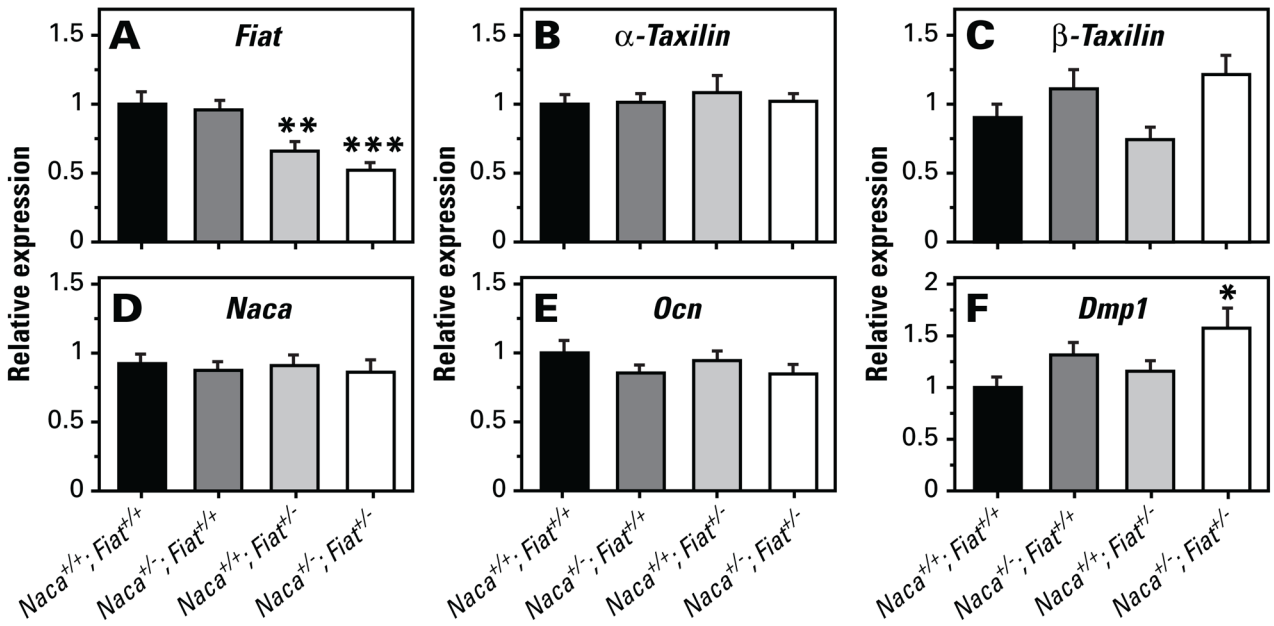

Fig. 3.

Gene expression monitoring. RNA was isolated from calvaria of 8 week-old mice (n=14 to 16 mice per group), reverse-transcribed, and analyzed by RT-qPCR. 18S ribosomal RNA was used as endogenous control, and expression levels are compared to $Naca^{+/+}$; $Fiat^{+/+}$ control mice which were arbitrarily ascribed a value of 1. A. *Fiat*. B. *α-taxilin*. C. *β-taxilin*. D. *Naca*. E. *Ocn*. F. *Dmp1*. *, $p<0.05$; **, $p < 0.01$, ***, $p<0.001$.

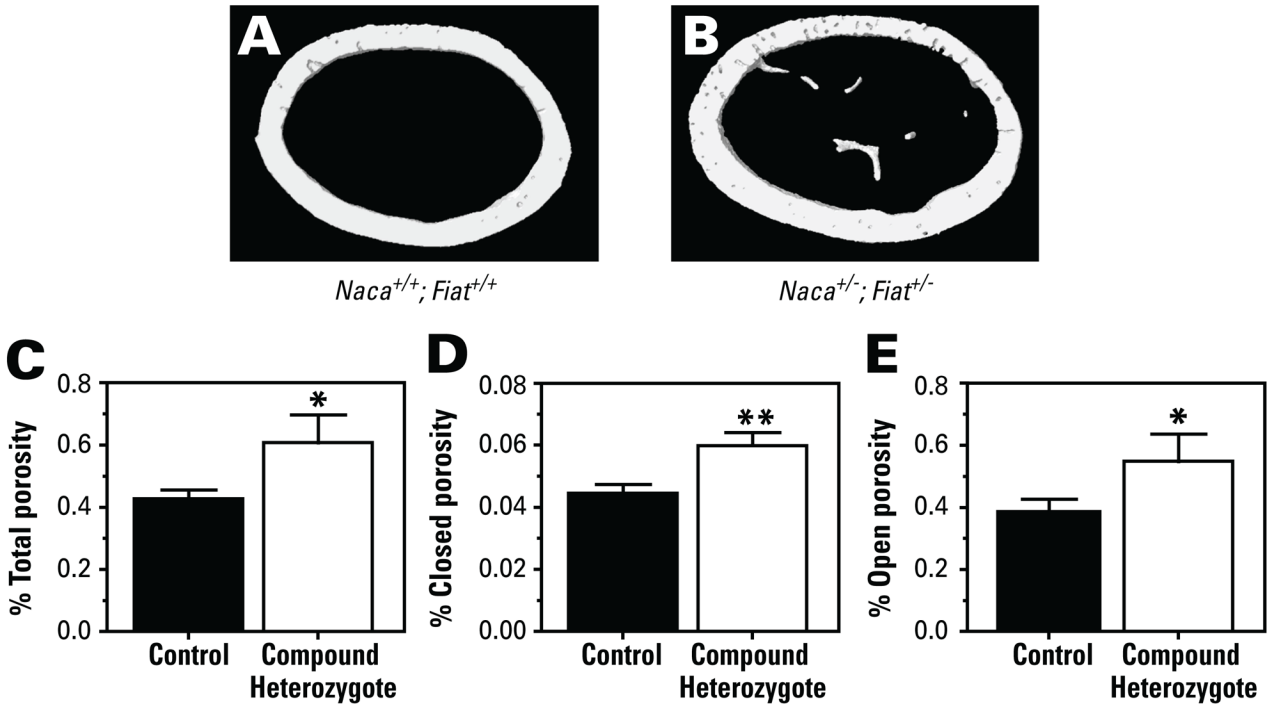

Fig. 4.

Increased porosity in femurs from compound heterozygous mice. A, B. Three-dimensional reconstructions of the cortical mid diaphysis. Representative images from a control (A, *Naca*$^{+/+}$; *Fiat*$^{+/+}$) and a compound heterozygote (B, *Naca*$^{+/-}$; *Fiat*$^{+/-}$) are shown. C–E. Cortical porosity measured using reconstructed images from μCT. Values for all control genotypes (*Naca*$^{+/+}$; *Fiat*$^{+/+}$, *Naca*$^{+/-}$; *Fiat*$^{+/+}$, *Naca*$^{+/+}$; *Fiat*$^{+/-}$) were highly homogeneous and results from these animals were grouped and expressed as ‘Control’. C. Total porosity. D. Closed porosity. E. Open porosity. *, $p<0.05$; **, $p < 0.01$.

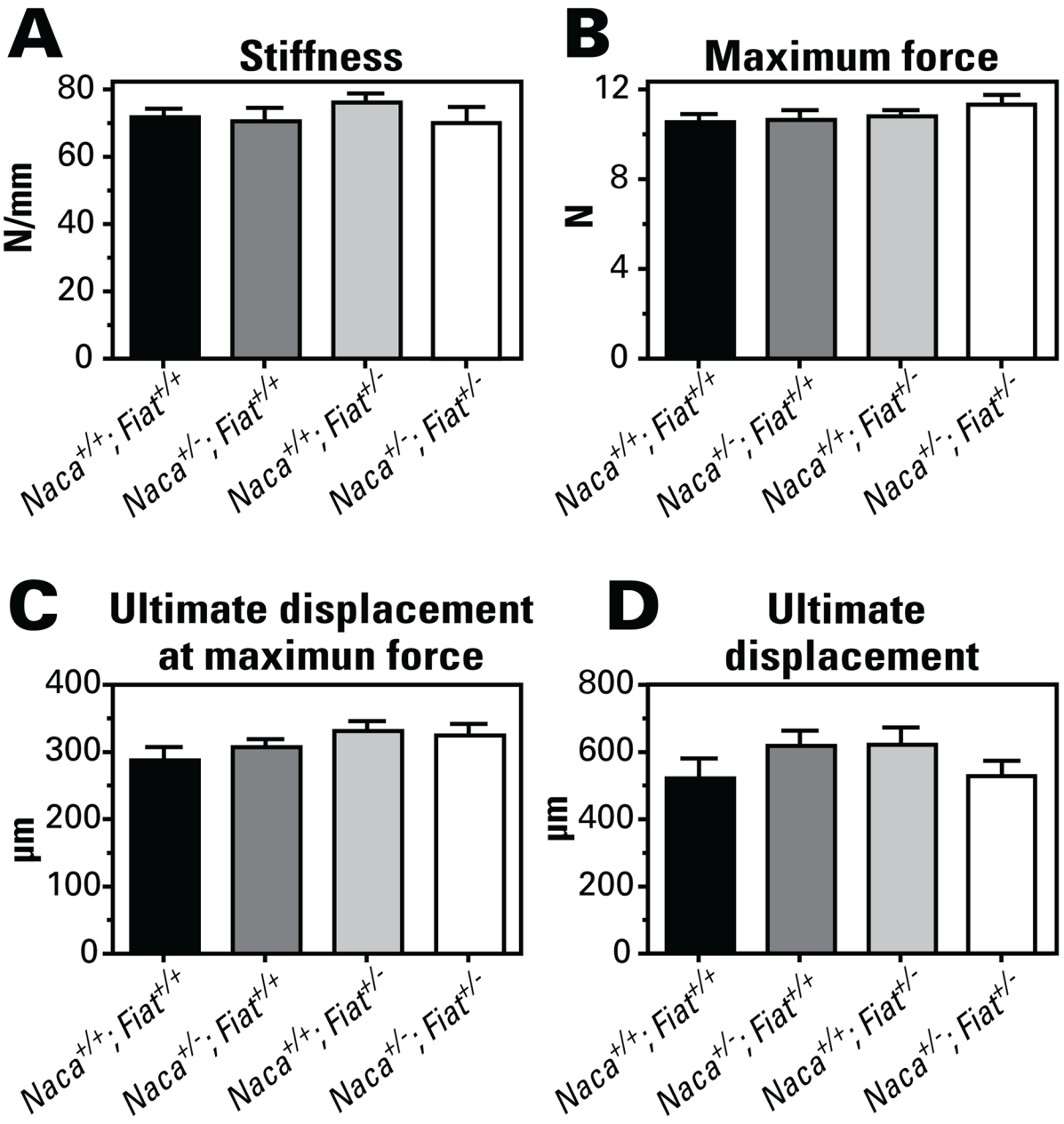

Fig. 5.

Bone biomechanical properties. Three-point bending tests revealed no changes in femoral stiffness (A), maximum force (B), ultimate displacement at maximum force (C), or ultimate displacement (D) between genotypes.

Table 1

Static histomorphometry

TRABECULAR PARAMETERS	*Naca*$^{+/+}$; *Fiat*$^{+/+}$	*Naca*$^{+/-}$; *Fiat*$^{+/+}$	*Naca*$^{+/+}$; *Fiat*$^{+/-}$	*Naca*$^{+/-}$; *Fiat*$^{+/-}$
BV/TV (%)	5.83±0.21	5.60±0.20	5.92±0.16	5.59±0.25
Trabecular number (1/mm)	1.70±0.04	1.64±0.05	1.70±0.04	1.64±0.07
Trabecular separation (μm)	248.0±3.70	250.0±3.00	247.2±3.00	250.0±4.80
Trabecular thickness (μm)	34.1±0.50	34.0±0.26	34.8±0.37	34.1±0.35
SMI	1.97±0.02	2.02±0.02	1.99±0.01	2.00±0.03
Connectivity density (1/mm^3)	196.4±7.04	184.1±8.52	199.2±6.08	194.4±15.22

CORTICAL PARAMETERS	*Naca*$^{+/+}$; *Fiat*$^{+/+}$	*Naca*$^{+/-}$; *Fiat*$^{+/+}$	*Naca*$^{+/+}$; *Fiat*$^{+/-}$	*Naca*$^{+/-}$; *Fiat*$^{+/-}$
Total tissue area (mm^2)	1.57±0.02	1.54±0.04	1.64±0.02	1.61±0.03
Cortical bone area (mm^2)	0.57±0.01	0.56±0.02	0.60±0.01	0.59±0.01
Cortical thickness (mm)	0.11±0.11	0.11±0.01	0.11±0.01	0.11±0.01